Fifth International Conference on Numerical Methods in Geomechanics / Nagoya / 1-5 April 1985

Numerical model for liquefaction problem under multi-directional shearing on horizontal plane

FUMIO YAMAZAKI
Shimizu Construction Co. Ltd, Tokyo, Japan

IKUO TOWHATA & KENJI ISHIHARA
University of Tokyo, Japan

ABSTRACT : A new effective stress model is developed for computing liquefaction potential of soil elements under multi-directional shearing. This model is composed of both deformation model with multiple non-linear springs and pore pressure model based on strain energy concept. Using this model, several series of numerical simulation of liquefaction for several loading patterns, such as a circular shear pattern, were conducted. Numerical results obtained by the model were in good agreements with laboratory test results in terms of stress-strain relation and pore water buildup during shear loading. Furthermore this effective stress model is embodied into the theory of wave propagation through two-phase media, and dynamic response analysis of horizontally layered ground under multi-directional shaking is made based on the effective stress method. This analytical procedure was applied to liquefaction study of a site in Niigata city devastated by the 1964 earthquake, and coupled effects of two horizontal motions on the dynamic response and liquefaction of the ground were examined.

1 INTRODUCTION

The shear stresses induced on soil elements in a horizontally layered ground during earthquake change in random manner not only in amplitude but also in direction. The effects of multi-directional shear loading on liquefaction potential have been previously examined experimentally by Seed, Pyke & Martin (1978), Ishihara & Yamazaki (1980), and Yamada & Ishihara (1983). Though there are some quantitative differences in multi-directional effects, these studies have equally demonstrated that liquefaction is more liable to occur under multi-directional loading than under uni-directional loading.

The multi-directional shearing on horizontal plane involves rotation of principal stress axes in three dimensional stress space as shown in Fig.1. Therefore numerical model for multi-directional shearing must be able to generate shear strain increment and pore water pressure increment even when octahedral shear stress, τ_{oct}, is kept constant as encountered in circular loading condition.

A new effective stress model meeting such a requirement is proposed herein. This model is composed of two sub-models i.e., deformation model and pore pressure model. The outline of the model and its use in the dynamic response analysis will be presented in the following pages.

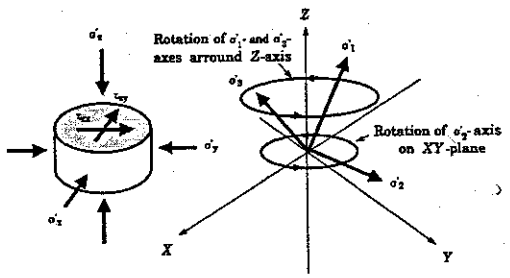

Fig.1 Rotation of the principal stress axes caused by multi-directional shearing

3 PORE PRESSURE MODEL

Prediction of pore water pressure change during multi-directional shearing is made by means of a revised version of the pore pressure model which is proposed by Towhata & Ishihara (1985).

Here we assumed that an experimental fact obtained from hollow cylindrical torsion tests is also valid in multi-directional shearing condition, that is "Excess pore water pressure is determined solely by accumulated shear strain energy and current values of shear stress of a soil element."

Thus equivalent shear strain energy surface of axisymmetric shape as shown in Fig.3 exsists in the three dimensional stress space which consists of two shear stresses, τ_{zx} and τ_{zy}, and effective vertical stress, σ'_z.

$$\tau_{zx}^2+\tau_{zy}^2=tan^2\phi'(\sigma'_z-\sigma'_{zk})^2-tan^2\phi'(\sigma'_{zp}-\sigma'_{zk})^2 \quad \cdots(14)$$

where ϕ' is angle of internal friction, σ'_{zp} is effective vertical stress when τ_{zx} and τ_{zy} are zero, σ'_{zk} is a parameter which is related with the shape of the equivalent shear strain energy surface and is defined by

$$\sigma'_{zk}=C_p\,\sigma'_{zp} \quad \cdots(15)$$

where C_p is a soil constant determined by laboratory tests.

A section view of the equivalent shear strain energy surface which includes σ'_z-axis is shown in Fig.4.

σ'_{zp} is determined by accumulated shear strain energy of a soil element of unit volume, W_s, which is defined by

$$W_s=\int_0^{\gamma_{zx}}\tau_{zx}\,d\gamma_{zx}+\int_0^{\gamma_{zy}}\tau_{zy}\,d\gamma_{zy} \quad \cdots(16)$$

Here we introduce empirical relations between W_s and excess pore water pressure at zero shear stress, u_0.

When $u_0/\sigma'_{z0}\leq 0.5$

$$\frac{u_0}{\sigma'_{z0}}=\frac{1}{1+\left(\dfrac{r}{(W_s/\sigma'_{z0})}\right)^{\alpha}} \quad \cdots(17)$$

When $0.5<u_0/\sigma'_{z0}\leq 1.0$

$$\frac{u_0}{\sigma'_{z0}}=\frac{\alpha}{4}\cdot\left(ln(W_s/\sigma'_{z0})-ln\,r\right)+0.5 \quad \cdots(18)$$

where σ'_{z0} is initial effective vertical stress, α and r are soil constants which are obtained by laboratory tests.

The relation expressed by Eqs.(17) and (18) is shown in Fig.5.

There is another relation as follows,

$$u_0=\sigma'_{z0}-\sigma'_{zp} \quad \cdots(19)$$

From Eqs.(14)~(19) we can obtain effective vertical stress at various stage of cyclic loadings, σ'_z, and the buildup of pore water pressure in general condition, u, is also obtained as follows,

$$u=\sigma'_{z0}-\sigma'_z \quad \cdots(20)$$

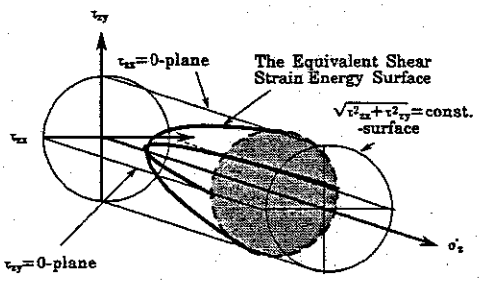

Fig.3 The equivalent shear strain energy surface defined in the stress space

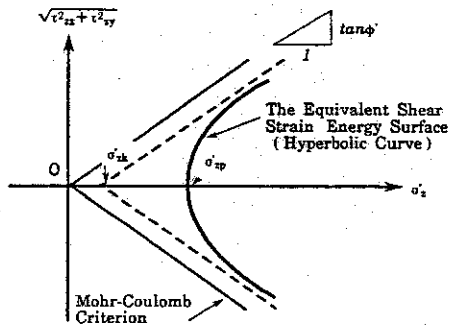

Fig.4 A section view of the equivalent shear strain energy surface

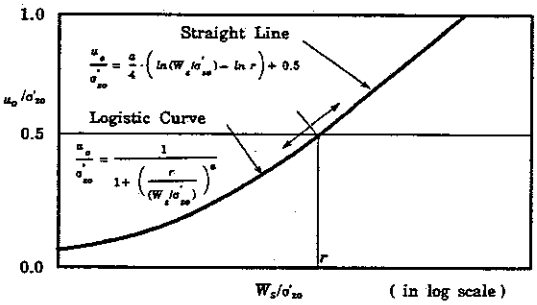

Fig.5 Relation between shear strain energy vs. pore water pressure at zero shear stress

2 STRESS VERSUS STRAIN MODEL

A stress-strain model for principal stress axes rotation in triaxial torsion shear stress condition proposed by Towhata & Ishihara (1985) is applied in multi-directional shearing problem with a few revisions.

This model called the multi-spring model consists of two rigid rings and numerous non-linear springs connected together as shown in Fig.2. When it represents a soil element, external forces are applied to the inner ring while the outer ring is fixed. The stress-strain matrix for the multi-spring model can be expressed in incremental form as follows,

$$\{d\tau\} = [D]\{d\gamma\} \qquad \cdots\cdots(1)$$

where $\{d\tau\}$ and $\{d\gamma\}$ are shear stress and shear strain increment vector of a soil element respectively, and they consist of two directional components on a horizontal plane.

$$\{d\tau\}^T = (d\tau_{zx}, d\tau_{zy}) \quad \{d\gamma\}^T = (d\gamma_{zx}, d\gamma_{zy}) \qquad \cdots(2)$$

Relation between force, f_θ, and deformation, x_θ, of each spring follows Ramberg-Osgood model with Masing rule.

Then for the initial virgin-loading phase,

$$f_\theta = \frac{k_t \cdot x_\theta}{1 + \alpha \left| \frac{f_\theta}{f_f} \right|^\beta} \qquad \cdots\cdots(3)$$

and for the unloading and the reloading phase,

$$f_\theta - f_{rev} = \frac{k_t \cdot (x_\theta - x_{rev})}{1 + \alpha \left| \frac{f_\theta - f_{rev}}{2 f_f} \right|^\beta} \qquad \cdots\cdots(4)$$

where x_{rev} and f_{rev} denote x_θ and f_θ at a turning point of loading direction respectively, k_t is initial shear modulus, f_f is shear strength, α and β are non-linear constants of the single spring.

These constants of the single spring are derived from soil constants expessed in the form of Ramberg-Osgood model, initial shear modulus, G_t, shear strength, τ_f, shear strain at failure, γ_f, damping ratio at large strain, h_{max}, as follows,

$$k_t = \frac{1}{\pi} G_t \qquad \cdots\cdots(5)$$

$$\alpha = \frac{\gamma_f}{\tau_f} G_t - 1 \qquad \cdots\cdots(6)$$

$$\beta = \frac{2\pi h_{max}}{2 - \pi h_{max}} \qquad \cdots\cdots(7)$$

$$f_f = \frac{k_t}{1+\alpha} C_r \gamma_f \qquad \cdots\cdots(8)$$

where C_r is correction factor of failure strains between the single spring and the multi-spring.

Shear stress of the multi-spring model is obtained by integrating the forces of a group of springs.

$$d\tau = \int_{-\pi}^{\pi} \mathbf{n} \cdot df_\theta \cdot d\theta \qquad \cdots\cdots(9)$$

$$\{n\}^T = (\cos\theta \ , \sin\theta \ ) \qquad \cdots\cdots(10)$$

where $\{n\}$ is a unit vector of coordinate transformation.

The force-deformation relation of each spring is approximated by a linear relationship as follows,

$$df_\theta = k_\theta (x_\theta) \cdot dx_\theta \qquad \cdots\cdots(11)$$

where $k_\theta(x_\theta)$ is the tangential shear modulus of one spring which can be obtained by differentiation of Eqs.(3) and (4).

The deformation increment of the individual spring which is located at angle θ is expressed in terms of the strain increment of the multi-spring model as,

$$dx_\theta = \{n\}^T \cdot \{d\gamma\} \qquad \cdots\cdots(12)$$

Introducing Eqs.(11) and (12) into Eq.(9), we obtain,

$$[D] = \int_{-\pi}^{\pi} k_\theta (x_\theta) \ \mathbf{n} \cdot \mathbf{n}^T \, d\theta \qquad \cdots\cdots(13)$$

The detailed explanation of the multi-spring model is described in another paper mentioned before.

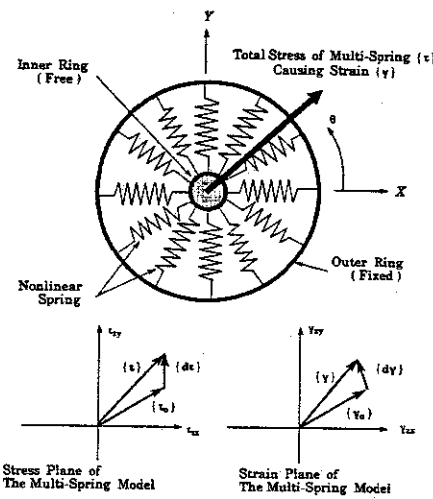

Fig.2 The multi-spring model and its stress and strain on a horizontal plane

4 NUMERICAL SIMULATION OF THE EFFECTIVE STRESS MODEL

New effective stress model is made up by combining the multi-spring model with the pore pressure model. The effective vertical stress computed by the pore pressure model is taken into account in the next step calculation as follows,

$$G_t = G_{to}(\sigma'_z/\sigma'_{zo})^{0.4} \quad \cdots\cdots(21)$$

$$\tau_f = \sigma'_z \tan\phi' \quad \cdots\cdots(22)$$

where G_{to} is initial shear modulus of soil before cyclic loading.

Numerical simulation of uni-directional cyclic simple shear tests on Toyoura sand of 40~50% relative density was conducted by the model. Soil constants used in the calculation are listed in Table 1.

Typical simulation results of a stress controlled undrained shear test are shown in Figs.6 and 7. Stress-strain relation and effective stress path are in good agreements with laboratory test results.

Series of numerical simulation for circular and elliptic shear loading pattern were also conducted. Typical numerical results in circular loading are shown in Figs.8~10.

Characteristic behavior of effective stress path in the circular simple shear tests, the suspension of the pore water pressure buildup when the stress path approach the failure surface, can be properly modeled in Fig.10.

The simulation results of circular and elliptic shear loadings are summarized in Fig.11 together with the results of uni-directional loading.

These results indicate that the resistance to liquefaction becomes smaller as the shear stress trace changes from the straight line to the ellipse and further to the circle. This tendancy coincides with the laboratory test results, multi-directional simple shear tests by Ishihara & Yamazaki (1980) and cubical triaxial tests by Yamada & Ishihara (1983).

Table 1. Soil constants of Toyoura sand used in the calculation

Intitial vertical stress; σ'_{zo}	294 kN/m^2
Intitial shear modulus; G_t	140,000 kN/m^2
Angle of internal friction; ϕ'	44°
Shear strain at failure; γ_f	0.03
Damping ratio at large strain; h_{max}	0.35
Correction factor of spring const.; C_r	0.80
Pore pressure coefficient; a	0.848
Pore pressure coefficient; r	2.04×10^{-3}
Pore pressure coefficient; C_p	0.05

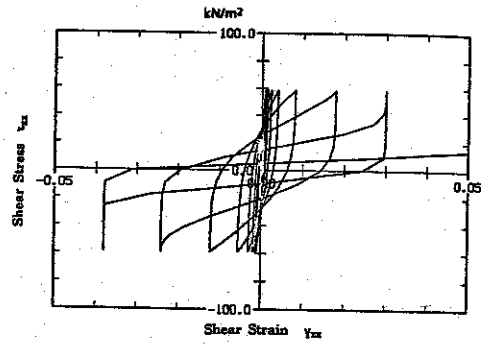

Fig.6 Stress-strain relation in uni-directional loading by the model

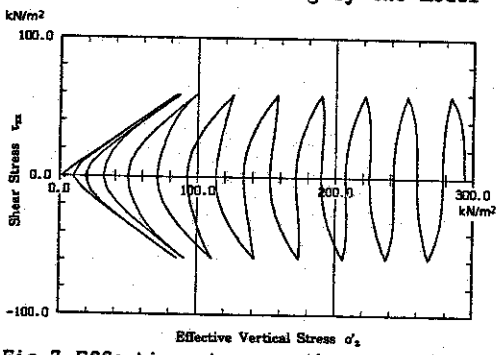

Fig.7 Effective stress path in uni-directional loading by the model

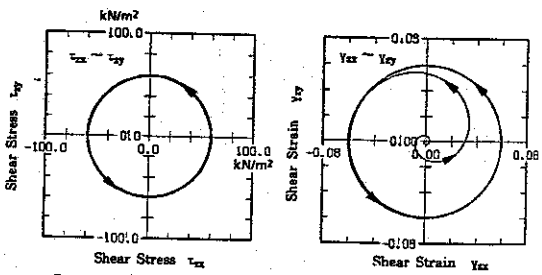

Fig.8 Traces of stress and strain in circular loading by the model

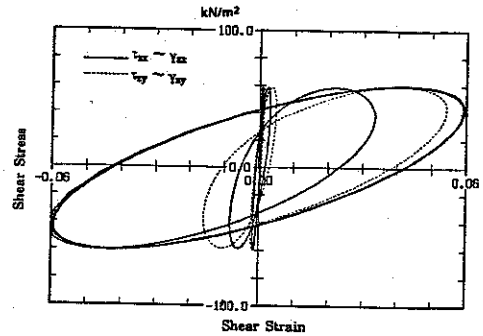

Fig.9 Stress-strain relation in circular loading by the model

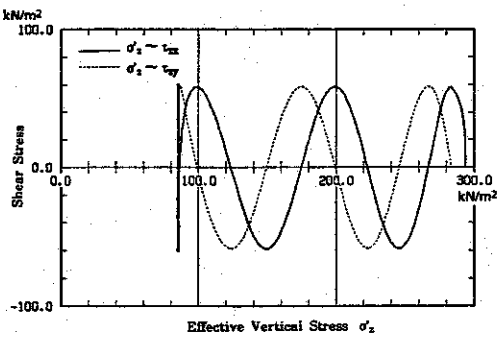

Fig.10 Effective stress path in circular loading by the model

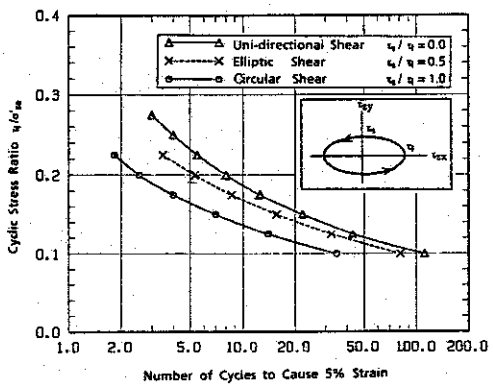

Fig.11 Relation between cyclic stress ratio vs. number of cycles to cause liquefaction by the model

5 BASIC EQUATIONS FOR EFFECTIVE STRESS ANALYSIS IN TWO-DIRECTIONAL HORIZONTAL MOTION

Dynamic effective stress analysis on saturated soil deposits in two-directional horizontal motion is developed. The method of analysis is the extension of the method of analysis for uni-directional horizontal motion presented previously by Ishihara & Towhata (1980).

General form of equations of motion for saturated porous media was originally developed by Biot. In the response analysis of a horizontally layered soil deposit, it is generally assumed that any stress and displacement component change only in the vertical z-direction. Therefore the equations of motion for solid phase are written as,

$$\rho_s \frac{\partial^2 u_x}{\partial t^2} = \frac{\partial \tau_{zx}}{\partial z} - b\left(\frac{\partial u_x}{\partial t} - \frac{\partial v_x}{\partial t}\right) \quad \cdots\cdots(23)$$

$$\rho_s \frac{\partial^2 u_y}{\partial t^2} = \frac{\partial \tau_{zy}}{\partial z} - b\left(\frac{\partial u_y}{\partial t} - \frac{\partial v_y}{\partial t}\right) \quad \cdots\cdots(24)$$

$$\rho_s \frac{\partial^2 u_z}{\partial t^2} = -\frac{\partial \sigma_z}{\partial z} - b\left(\frac{\partial u_z}{\partial t} - \frac{\partial v_z}{\partial t}\right) + \rho_s \cdot g \quad \cdots(25)$$

in which u_i and v_i denote the displacements of the solid phase and the fluid phase in the i-direction respectively, ρ_s is the bulk mass density of the solid phase, g is the gravitational accerleration, and b denotes a constant related to the permeability, k, porosity, n, and the unit weight of water, γ_w, in the following way,

$$b = \frac{n^2 \gamma_w}{k} \quad \cdots\cdots(26)$$

The equations of motion for fluid phase are given by,

$$\rho_w \frac{\partial^2 v_x}{\partial t^2} = b\left(\frac{\partial u_x}{\partial t} - \frac{\partial v_x}{\partial t}\right) \quad \cdots\cdots(27)$$

$$\rho_w \frac{\partial^2 v_y}{\partial t^2} = b\left(\frac{\partial u_y}{\partial t} - \frac{\partial v_y}{\partial t}\right) \quad \cdots\cdots(28)$$

$$\rho_w \frac{\partial^2 v_z}{\partial t^2} = -\frac{\partial p}{\partial z} + b\left(\frac{\partial u_z}{\partial t} - \frac{\partial v_z}{\partial t}\right) + \rho_w \cdot g \quad \cdots(29)$$

in which ρ_w is the bulk mass density of the fluid phase, p denotes the compressive stress acting on the fluid portion.

Assuming that the seepage flow in the horizontal x- and y-directions does not occur in the type of liquefaction problem for the horizontal soil deposit,

$$u_x = v_x \ , \quad u_y = v_y \quad \cdots\cdots(30)$$

Through the introduction of the first equation of these identity relations in the Eqs.(23) and (27), and adding both, we obtain,

$$\rho \frac{\partial^2 u_x}{\partial t^2} = \frac{\partial \tau_{zx}}{\partial z} \quad \cdots\cdots(31)$$

$$\rho = \rho_s + \rho_w \quad \cdots\cdots(32)$$

where ρ is the unit mass of the soil including the solid and fluid phase.

In the same manner, we can get another equation for horizontal y-direction,

$$\rho \frac{\partial^2 u_y}{\partial t^2} = \frac{\partial \tau_{zy}}{\partial z} \quad \cdots\cdots(33)$$

Eqs.(31) and (33) are equations of shear wave propergation in the vertical z-direction. Since the soild phase and the fluid phase move together in horizontal direction, it is sufficient to solve Eqs.(31) and (33) which represent the motion of the both phases.

As the water flow is assumed to occur only in the vertical direction in this study, equations of motion and seepage in the vertical direction are identical to those of previous study for one dimensional problem as follows,

$$\frac{\gamma_t}{g}\frac{\partial W}{\partial t}+\frac{\gamma_w}{g}\frac{\partial Q}{\partial t}=-\frac{\partial \sigma}{\partial z}+\gamma_t \qquad \cdots\cdots(34)$$

$$\frac{n\gamma_w}{g}\frac{\partial W}{\partial t}+\frac{\gamma_w}{g}\frac{\partial Q}{\partial t}+\frac{b}{n}Q+n\frac{\partial u}{\partial z}-n\gamma_w=0 \qquad \cdots\cdots(35)$$

$$\frac{\partial W}{\partial z}+\frac{\partial Q}{\partial z}=0 \qquad \cdots\cdots(36)$$

$$\frac{\partial W}{\partial z}=m_v\left(-\frac{\partial \sigma}{\partial z}+\frac{\partial u}{\partial t}-\frac{\partial u_g}{\partial t}\right) \qquad \cdots\cdots(37)$$

where W is the vertical velocity of the soil skelton, Q is the vertical velocity of water relative to the soil skelton, σ and u denote the vertical total stress and the pore water pressure respectively, m_v is the coefficient of volume compressibility, u_g is the internally generated pore water pressure evaluated with the use of the pore pressure model.

6 NUMERICAL INTEGRATIONS

The horizontal motions of soil stratum are determined by integrating Eqs.(31) and (33) with reference to the stress-strain relation given by the multi-spring model.

In carrying out the step-by-step integration with respect to time, the stress-strain relationship in a small time inteval is approximated as follows,

$$\{\tau\}=\{\tau_0\}+[D]\{\gamma-\gamma_0\} \qquad \cdots\cdots(38)$$

in which $\{\tau_0\}$ and $\{\gamma_0\}$ denote shear stress and shear strain vector at time t_0, [D] can be obtained by numerical integration of Eq.(13) and written as,

$$[D]=\begin{bmatrix} d_{xx} & d_{xy} \\ d_{xy} & d_{yy} \end{bmatrix} \qquad \cdots\cdots(39)$$

Introducing Eqs.(38) and (39) into Eqs.(31) and (33) together with the relations, $\gamma_{zx}=\partial u_x/\partial z$ and $\gamma_{zy}=\partial u_y/\partial z$, we get,

$$\rho\frac{\partial^2 u_x}{\partial t^2}=d_{xx}\frac{\partial^2 u_x}{\partial z^2}+d_{xy}\frac{\partial^2 u_y}{\partial z^2}+\frac{\partial}{\partial z}\left(\tau^0_{zx}-d_{xx}\gamma^0_{zx}-d_{xy}\gamma^0_{zy}\right) \qquad \cdots\cdots(40)$$

$$\rho\frac{\partial^2 u_y}{\partial t^2}=d_{yy}\frac{\partial^2 u_y}{\partial z^2}+d_{xy}\frac{\partial^2 u_x}{\partial z^2}+\frac{\partial}{\partial z}\left(\tau^0_{zy}-d_{yy}\gamma^0_{zy}-d_{xy}\gamma^0_{zx}\right) \qquad \cdots\cdots(41)$$

in which upper suffix ^{0} refers to the variable at time t_0.

In order to carry out integration with respect to the depth, z, the horizontal sand deposit is divided into a number of layers. These layers are converted to a lumped mass system as shown in Fig.12 in which the masses are connected by the multi-spring model.

Input motion of two horizontal components is applied to the lowest mass through viscous boundary.

Applying Eqs.(40) and (41) to each layer of the deposit, we obtain two differential equations for each lumped mass. These sets of equations are rewritten as follows,

$$[M]\{\ddot{u}\}+[C]\{\dot{u}\}+[K]\{u\}=\{f\} \qquad \cdots\cdots(42)$$

in which $\{u\}$ is the displacement vector of the lumped mass system with $2\times(n+1)$-degree-of-freedam, $\{f\}$ is the force vector, [M] is the lumped mass matrix, [C] is the viscous damping matrix, [K] is the stiffness matrix. The numerical integration with time is made stepwise using the Newmark's β method with $\beta=1/4$.

For dissipation of pore water pressure in vertical direction, Eqs.(34)~(37) are numerically integrated stepwise using the method of weighted residuals.

At each small time interval, the dynamic response analysis for horizontal motion and the seepage analysis in vertiacal direction are conducted in turn.

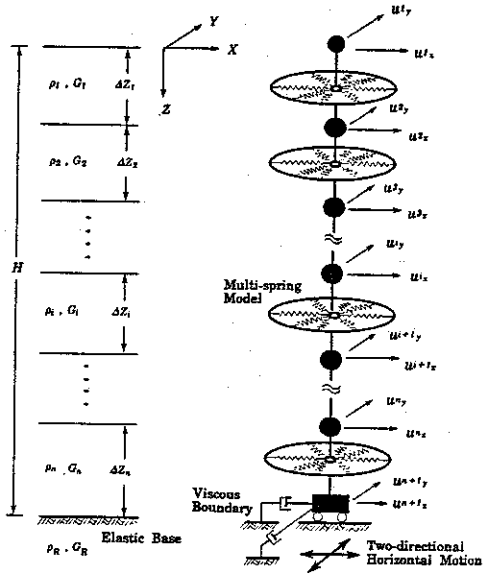

Fig.12 Model for dynanic response analysis in two-directional horizontal motion

7 ANALYSIS OF A SITE IN NIIGATA CITY DURING THE 1964 EARTHQUAKE

The method of dynamic response analysis was applied to a liquefaction study of Kawagishi-cho site in Niigata city in order to clarify the coupled effect of two horizontal motions on dynamic response and liquefaction of the ground.

During the Niigata earthquake of 1964, signs of liquefaction were observed around this site modeled in Fig.13. Soil parameters were determined by the soil investigations using Osterberg sampler and the laboratory tests for undisturbed samples. The pore pressure coefficient, r, was determined from the cyclic stress ratio obtained by triaxial tests, R'_{20}, considering K_0 condition.

The acceleration records obtained in the basement of a building in Akita city at the time of 1964 earthquake were rescaled to have appropriate predominant peoriod and maximum amplitude. These modified motions, whose maximum amplitudes are 60 gal in NS-direction and 53 gal in EW-direction, were used as incident waves at the base layer.

The dynamic effective stress analyses in two-directional motion and in uni-directional motion were conducted. Results of those analyses are shown in Figs.14~19.

In case of two-directional analysis, liquefaction occured in the loose layer at GL-10m~-12m. On the other hand, in case of uni-directional analyses, maximum pore water pressures developed in the same layer were 85% and 92% of the initial effective vertical stress by EW motion and by NS motion respectively.

Accelerations of the ground surface by two-directional analysis were decreasing in accordance with the pore pressure buildup in the loose layer. Maximum accelerations by two-directional analysis were smaller than those by uni-directional analyses because non-linearities of the loose layer were intensified by the combined motion. Such effects were also observed in short-period range of the acceleration response spectra in Fig.15.

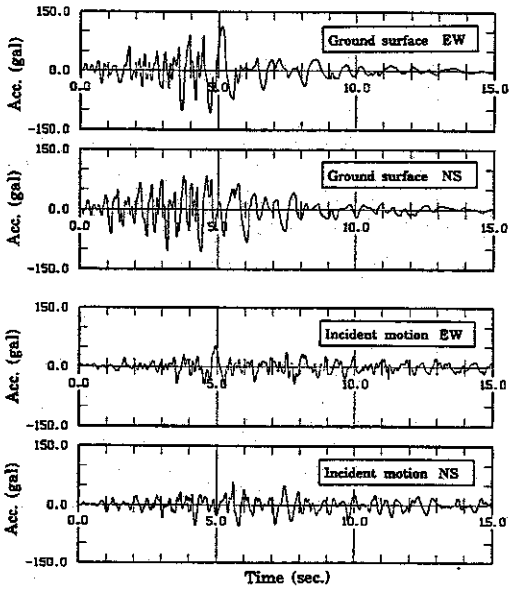

Fig.14 Computed acceleration time histories by two-directional analysis

Depth (m)	Layer div.	γ_t (kN/m³)	Poro-city n	K_{ur} value	G_i ($\times 10^2$ kN/m²)	m_v ($\times 10^{-2}$ m²/kN)	ϕ' (degree)	Cyclic Strength R_{20}	r ($\times 10^{-2}$)
0	1	13	0.52	0.5	69	—	38	—	—
	2	"	"	"	52	—	37	—	—
5	3	18	0.53	"	46	1.91	34	0.17	0.71
	4	"	"	"	"	1.69	"	"	0.72
	5	19	0.47	0.6	120	1.54	39	0.20	1.14
	6	"	"	"	150	1.42	41	0.22	1.34
	7	"	"	"	"	1.34	"	"	1.34
10	8	"	"	"	"	1.29	"	0.19	0.77
	9	"	"	"	"	1.22	"	0.16	0.39
	10	"	"	"	"	1.17	"	0.22	1.35
	11	"	"	"	"	1.13	"	0.21	1.14
15	12	20	0.41	0.7	320	1.10	47	0.30	0.73
	13	"	"	"	"	1.05	"	0.29	2.89
	14	21	0.35	0.8	430	0.989	51	0.33	4.22
20	15	"	"	"	"	0.927	"	0.31	3.46
25	16	"	"	"	480	0.872	52	0.32	3.49
	17	"	"	"	640	0.831	55	0.35	3.67
30	Base	Soil constants below are adapted for all layers. $k=1.0\times10^{-2}$, $\gamma_w=0.03$, $h_{max}=0.35$, $C_v=0.90$, $\alpha=0.848$, $C_g=0.05$ Soil constans of base rock ; $\gamma_t=20$kN/m², shear wave velocity, $V_s=600$m/sec							

Fig.13 Soil properties used for the analysis of Kawagishi-cho site

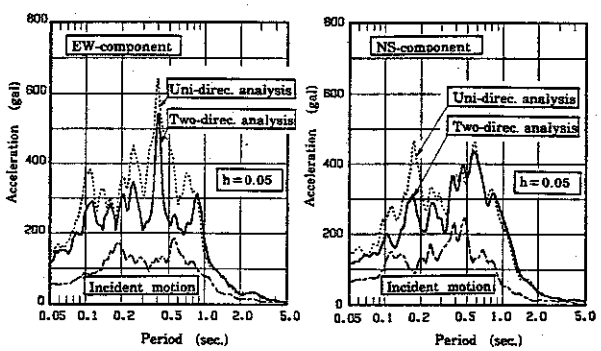

Fig.15 Computed acceleration response spectra of the ground surface

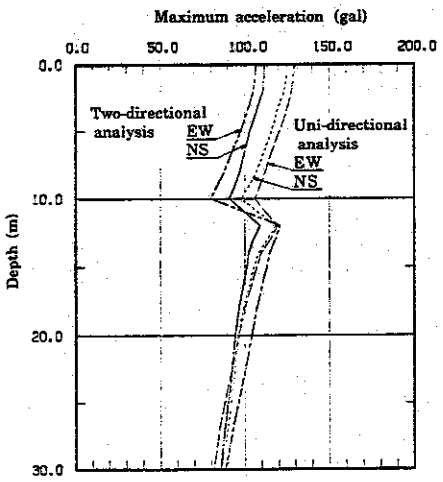

Fig.16 Distributions of the computed maximum accelerations

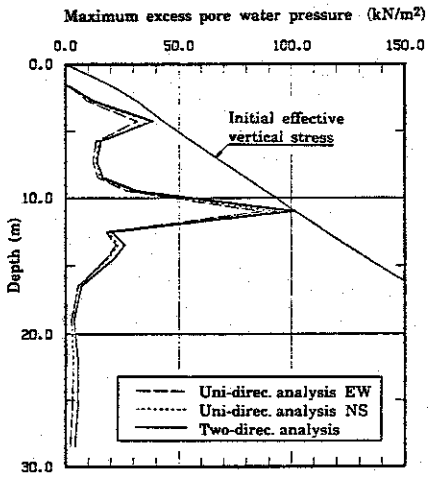

Fig.17 Distributions of the computed maximum pore water pressures

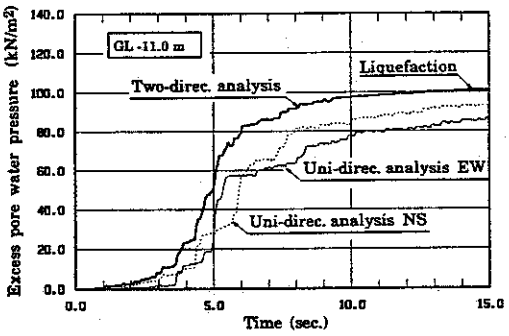

Fig.18 Computed time histories of pore water pressures in the loose layer

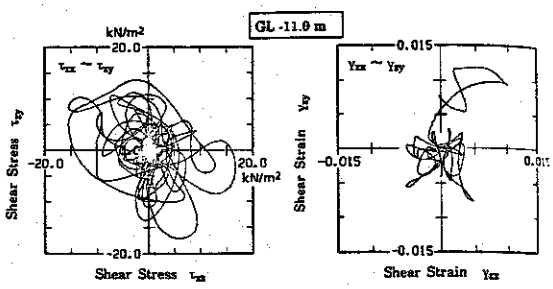

Fig.19 Traces of stress and strain by two-directional analysis in the loose layer

8 CONCLUSION

A new effective stress model which is composed of the multi-spring model and the pore pressure model is developed for liquefaction analysis of soil elements under multi-directional shearing.

Results of numerical simulation for several loading patterns were in good agreements with laboratory test results in terms of stress-strain relation and pore water pressure buildup.

Furthermore, the dynamic response analysis of horizontally layered ground for multi-directional shaking is developed based on the effective stress method by introducing the proposed model.

This method was applied to liquefaction analysis of Kawagishi-cho site in Niigata city during 1964 earthquake. The results of analysis showed that combined two-directional incident motion is more liable to cause liquefaction but induces smaller acceleration response than uni-directional incident motion.

REFERENCES

Seed,H.B.,Pyke,R.M. & Martin,G.R. 1978. Effect of multi-directional shaking on pore pressure development in sands. Proc. ASCE GT1 Vol.104:27-44

Ishihara,K. & Yamazaki,F. 1980. Cyclic simple shear tests on saturated sand in multi-directional loading. Soils and Foundations Vol.20 No.1:45-59

Yamada,Y. & Ishihara,K. 1983. Undrained deformation characteristcs of sand in multi-directional shear. Soils and Foundations Vol.23 No.1:61-79

Ishihara,K. & Towhata,I. 1980. One-dimensional soil response analysis during earthquakes based on effective stress method. Jour. of Facu. of Eng. The Univ. of Tokyo (B) Vol 35 No.4:655-700

Towhata,I. & Ishihara,K. 1985. Modeling soil behavior under principal stress axes rotation. Proc. of 5th ICONMIG